Lecture 03

Information Carriers and the Earth's Atmosphere

AST-B09 Observational Astronomy

Rogério Monteiro-Oliveira, Ph.D. (孟羅傑)

Goals of Lecture 03

This lecture establishes the physical mechanics of astronomical information carriers and formalizes the degradative effects of the Earth's atmosphere on astronomical observations. Moving from the vacuum of space to the telescope pupil, its primary objectives are to:

- Introduce the Multimessenger Paradigm, focusing on electromagnetic radiation, photon statistics, and the fundamental principles of radiative transfer.
- Characterize the Earth's atmosphere as a participating physical medium, detailing its vertical thermodynamic structure and chemical composition.
- Systematically categorize and model the atmosphere's primary degradative effects on incoming light: absorption, emission, refraction, scattering, and macroscopic turbulence.
- Outline the practical observational strategies and physical criteria used to mitigate these atmospheric effects, ranging from differential background subtraction techniques to geographic site selection.

Contents

1 The Multimessenger Paradigm: Physics of Information Carriers

As established in Lecture 01, an observation is a continuous physical process where a signal is transported from a causally disconnected target to the observer via a propagation medium. Astronomy has evolved from a purely optical science into the era of **multimessenger astronomy**, which utilizes four distinct physical carriers to construct a panchromatic and complete view of the universe.

While the universe broadcasts information through all four carriers, their interaction with the Earth's environment dictates how we must observe them. Neutrinos, cosmic rays, and gravitational waves offer unique, non-photonic windows into the cosmos, but their detailed physical treatment and detection mechanisms will be the subject of a dedicated future lecture. Briefly:

- **Neutrinos:** Neutrinos are neutral, nearly massless elementary particles that interact with baryonic matter so weakly that they can pass through virtually anything. Because their probability of colliding with other particles is phenomenally small, the average distance they can travel before an interaction is immense. This allows them to shoot straight out of incredibly dense environments (like the nuclear furnaces of stellar cores or collapsing supernovae) completely unaltered. As a result, they act as pristine messengers, delivering unadulterated information directly from the deep interiors of these astrophysical engines.
- **Cosmic Rays:** Cosmic rays are highly energetic, massive particles traveling at near light-speed, primarily consisting of protons, electrons, and heavy atomic nuclei. Crucially, unlike photons or neutrinos, cosmic rays carry an electric charge. As they travel through the cosmos, their trajectories are continuously bent and deflected by the magnetic fields that permeate interstellar and intergalactic space. Because of this magnetic scattering, standard cosmic rays do not travel in straight lines and do not point back to their origins, effectively destroying our ability to pinpoint their sources unless the particles possess extraordinarily high energies.
- **Gravitational Waves:** Gravitational waves are physical ripples in the very fabric of spacetime itself, generated by the violent acceleration of massive, asymmetric systems (such as orbiting pairs of black holes or neutron stars). Unlike traditional telescopes that measure the deposited energy or power of incoming light, gravitational wave observatories directly measure the fundamental "strain", the minute stretching and squeezing of space as the wave passes through Earth. Because our detectors measure this actual amplitude rather than its diluted power, our sensitivity to these events drops off much more slowly with distance, which vastly increases the observable volume of the universe.

1.1 Electromagnetic Radiation (Photons) and the EM Spectrum

Despite the rise of multimessenger astronomy, photons remain the primary and most ubiquitous information carrier. Photons are quantized, massless spin-1 bosons that propagate at the speed of light (c). They exhibit a fundamental wave-particle duality, characterized by their energy $E = h\nu$, momentum $p = E/c$, and wavelength $\lambda = c/\nu$.

As illustrated in Figure 1, the astronomical **Electromagnetic (EM) Spectrum** spans over 20 orders of magnitude in frequency. Because the interaction of light with matter is strictly quantized, different observational bands are not merely human constructs; they trace entirely different physical, thermal, and non-thermal astrophysical processes:

- **Radio ($\lambda > 1$ mm):** Dominated by non-thermal emission (synchrotron radiation from relativistic electrons spiraling in magnetic fields), thermal bremsstrahlung (free-free emission in ionized plasmas), and the 21-cm hyperfine transition of neutral Hydrogen ($H\,I$).
- **Infrared / Sub-millimeter ($1\,\mu$m $< \lambda < 1$ mm):** The regime of "cold" the universe. Traces thermal continuum emission from interstellar dust ($T \sim 10 - 100$ K) and complex ro-vibrational transitions of molecules (e.g., CO, H_2O).
- **Optical / Ultraviolet (10 nm $< \lambda < 1\,\mu$m):** Traces thermal blackbody emission from stellar photospheres ($T \sim 3000 - 50,000$ K) and bound-bound electronic transitions in atoms and ions.
- **X-Ray / Gamma-Ray ($\lambda < 10$ nm):** The high-energy, violent universe. Traces million-degree plasmas (e.g., galaxy clusters), inverse-Compton scattering, matter falling into black hole accretion disks, and nuclear decay.

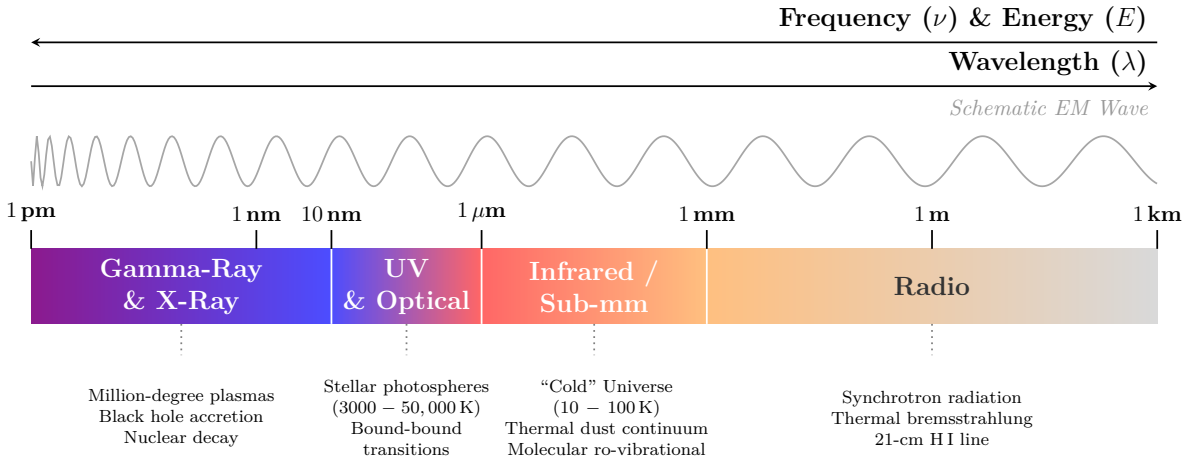

Figure 1: The astronomical Electromagnetic (EM) Spectrum. Observational bands represent distinct physical and thermal processes. The sine wave illustrates the continuous change in frequency and wavelength across the spectrum.

1.1.1 Macroscopic Description: Specific Intensity and Radiative Transfer

To extract physical meaning from these photons, we must rigorously define the radiation field. The fundamental macroscopic quantity in astrophysics is the **specific intensity**, I_ν. It is defined as the amount of energy dE crossing a differential area dA, within a solid angle $d\Omega$, in a frequency range $d\nu$, over a time dt:

$$dE = I_\nu \cos\theta \, dA \, d\Omega \, d\nu \, dt \tag{1}$$

where θ is the angle between the ray and the normal to dA. The units of I_ν are erg s^{-1} cm^{-2} Hz^{-1} sr^{-1}. A profound property of specific intensity is that I_ν *is strictly conserved along a ray in a vacuum.* Surface brightness does not diminish with distance.

However, the universe (and our atmosphere) is not a perfect vacuum. As the beam propagates through a medium, intensity is added by local emission (j_ν) and removed by local absorption (α_ν). This is described by the **Radiative Transfer Equation**:

$$\frac{dI_\nu}{ds} = j_\nu - \alpha_\nu I_\nu \tag{2}$$

By introducing the **optical depth** $d\tau_\nu = \alpha_\nu ds$ and the **source function** $S_\nu = j_\nu/\alpha_\nu$, the equation can be integrated to yield the formal solution of radiative transfer:

$$I_\nu(\tau_\nu) = I_\nu(0)e^{-\tau_\nu} + \int_0^{\tau_\nu} S_\nu(\tau'_\nu)e^{-(\tau_\nu - \tau'_\nu)} d\tau'_\nu \tag{3}$$

The first term represents the exponential attenuation of the original background source, while the second term represents the new light emitted by the intervening medium itself.

1.1.2 Photon Statistics: The Dual Nature of Light in Detectors

Because photons are bosons, their arrival times at a detector are not completely independent; they fundamentally follow Bose-Einstein statistics. The variance in the number of detected photons n in a given state reveals exactly how light behaves across different wavelengths:

$$\langle (\Delta n)^2 \rangle = \langle n \rangle + \langle n \rangle \left(\frac{1}{e^{h\nu/kT} - 1} \right) \tag{4}$$

Written this way, we can see that the total noise is the sum of two distinct physical effects. The first term ($\langle n \rangle$) represents discrete, random **particle-like noise**. The second term represents classical **wave-like bunching noise**.

This equation dictates a profound dichotomy in how we observe the universe:

- **The Optical/UV Regime (Particle Limit):** At high frequencies ($h\nu \gg kT$), a single photon carries much more energy than the thermal background. The exponential term in the denominator becomes massive, driving the entire wave-noise term to zero. Photons arrive randomly and independently, like discrete raindrops. The statistics reduce purely to standard **Poisson statistics**: $\langle (\Delta n)^2 \rangle \approx \langle n \rangle$. Therefore, the fundamental, inescapable limit of optical observations is Poisson shot noise, which scales simply as $\sqrt{n}$.

- **The Radio Regime (Wave Limit):** Conversely, at very low frequencies ($h\nu \ll kT$, in the Rayleigh-Jeans tail), photons have very little energy and are incredibly abundant. The denominator becomes very small, making the second term (the wave-noise term) dominant. The variance becomes $\langle(\Delta n)^2\rangle \approx \langle n\rangle^2$. Here, light behaves as a continuous electromagnetic wave. The photons tend to "bunch" together in phase, and the uncertainty is dominated by the fluctuations of the wave amplitude itself rather than the counting of discrete particles.

1.2 Transitioning from Vacuum to Medium

While photons travel largely unimpeded through the vacuum of interstellar space, their defining characteristic (unlike neutrinos or gravitational waves) is their strong electromagnetic interaction with baryonic matter. When these photons finally reach Earth after a journey of millions of years, they do not strike our telescope mirrors immediately.

Instead, they must first navigate a dense, turbulent, and chemically complex fluid: the Earth's atmosphere. Looking at the formal solution to the radiative transfer equation (Eq. 3), the atmosphere acts simultaneously as a profound absorber ($e^{-\tau_\nu}$) and a bright, contaminating source function (S_ν). This interaction profoundly alters the incoming EM spectrum, dictating not only *how* we observe, but *where* we must build our observatories to capture specific wavelengths.

2 The Earth's Atmosphere as a Propagation Medium

Before reaching a ground-based telescope, astrophysical information carriers must pass through the Earth's atmosphere. Rather than a passive void, the atmosphere is a stratified, participating fluid medium governed by complex thermodynamics, chemistry, and fluid dynamics. To fully understand its degradative effects (**extinction, emission, refraction, and turbulence**) we must first construct a rigorous physical model of its vertical structure and chemical composition.

Specifically, we can categorize these atmospheric effects and properties into five core topics:

- Atmospheric Layers
- Absorption
- Emission
- Scattering, Refraction & Dispersion
- Turbulence & Seeing

2.1 Atmospheric Layers: Vertical Structure and Thermodynamics

To a first approximation, the Earth's atmosphere behaves as an ideal gas in hydrostatic equilibrium. The pressure gradient precisely balances the downward gravitational force:

$$\frac{dP}{dz} = -\rho g \tag{5}$$

Using the ideal gas law $P = \frac{\rho kT}{\mu m_H}$ (where μ is the mean molecular weight and m_H is the mass of hydrogen), we can express the density gradient as:

$$\frac{dP}{P} = -\frac{\mu m_H g}{kT} dz = -\frac{dz}{H(z)} \tag{6}$$

Here, $H(z) = \frac{kT}{\mu m_H g}$ is the **pressure scale height**. Assuming an isothermal atmosphere ($T \approx 273$ K), the scale height is roughly constant at $H \approx 8$ km. Integrating this yields the barometric formula, showing that atmospheric pressure and density decay exponentially with altitude:

$$P(z) = P_0 e^{-z/H} \quad \text{and} \quad \rho(z) = \rho_0 e^{-z/H} \tag{7}$$

However, the atmosphere is *not* strictly isothermal. The vertical temperature gradient, or **lapse rate** ($\Gamma = -dT/dz$), dictates the atmosphere's primary structural layers (shown in Figure 2a), while the transition from turbulent mixing to molecular diffusion dictates its compositional regimes (Figure 2b). These layers directly impact astronomical observations:

1. **Troposphere (0 to $\approx$ 12 km):** The lowest layer, characterized by a positive lapse rate ($\Gamma \approx 6.5$ K/km) where temperature drops with altitude. Because the ground heats the air from below, the troposphere is thermodynamically unstable, driving massive convective currents and wind shear. This layer contains $\sim$ 75% of the atmospheric mass, nearly all of the water vapor, and is the exclusive birthplace of the turbulent cells that cause astronomical "seeing".

2. **Stratosphere ($\approx$ 12 to 50 km):** Here, the temperature *increases* with altitude ($\Gamma < 0$), creating a highly stable temperature inversion. This heating is driven entirely by the absorption of solar ultraviolet (UV) radiation by the ozone (O_3) layer. This stability halts the vertical convection from the troposphere.

3. **Mesosphere ($\approx$ 50 to 85 km):** Temperature again drops with altitude, reaching the coldest point in the atmosphere ($\sim$ 180 K) at the mesopause. Meteoroids typically ablate in this layer, leaving metallic ions (Na, Fe) that are occasionally used to reflect lasers for artificial guide star Adaptive Optics.

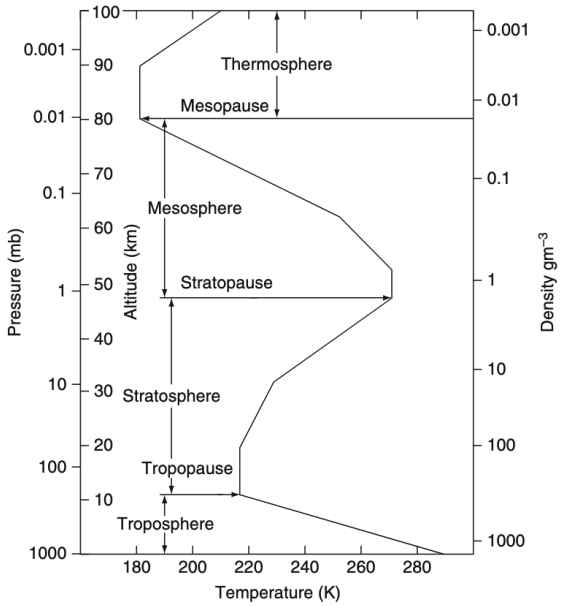

(a) The vertical temperature profile and structural stratification of the Earth's atmosphere. The environmental lapse rate (Γ) dictates the boundaries of the layers. Note that the thermodynamically unstable troposphere hosts the vast majority of water vapor and turbulent cells responsible for astronomical seeing, while the stratosphere maintains extreme stability due to UV absorption by the ozone layer.

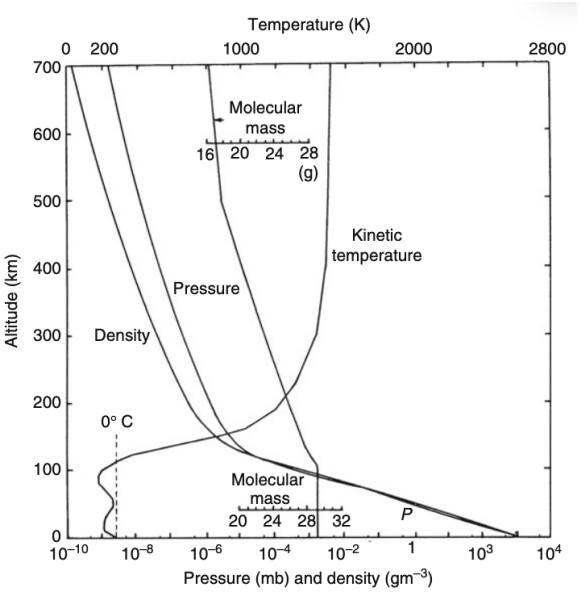

(b) The compositional stratification of the Earth's atmosphere. Below the turbopause ($\sim$ 100 km), macroscopic turbulent mixing governs fluid dynamics, maintaining a homogenous mixture of dry gases in the homosphere. Above the turbopause, in the heterosphere, the mean free path of molecules increases to the point where molecular diffusion dominates, causing gases to gravitationally stratify strictly according to their molecular weights.

Figure 2: Physical and compositional structure of the Earth's atmosphere. Figure from [1].

4. **Thermosphere / Ionosphere ($>$ 85 km):** High-energy solar extreme ultraviolet (EUV) and X-ray radiation photoionizes the sparse atomic oxygen and nitrogen, creating a plasma. The electron density N_e in this layer dictates the plasma frequency, which violently reflects low-frequency astronomical radio waves back into space. Furthermore, at an altitude of $\sim$ 100 km (the **turbopause**), the atmosphere transitions from the well-mixed homosphere into the heterosphere (see Figure 2b), where gases undergo gravitational stratification based solely on their molecular weights.

2.2 Absorption: Chemical Composition and Precipitable Water Vapor

The atmosphere's interaction with incoming electromagnetic radiation is strictly governed by its chemical composition and the molecular structure of its constituents. By volume, the dry atmosphere is highly homogeneous up to the turbopause ($\sim$ 100 km), consisting

primarily of inert homonuclear diatomics and noble gases: Nitrogen (N_2, 78.1%), Oxygen (O_2, 20.9%), and Argon (Ar, 0.9%). Because N_2 and O_2 are perfectly symmetrical, they lack a permanent electric dipole moment. Consequently, their vibrational and rotational transitions do not couple efficiently with electromagnetic fields, rendering the bulk of the dry atmosphere largely transparent in the infrared (IR) and sub-millimeter regimes.

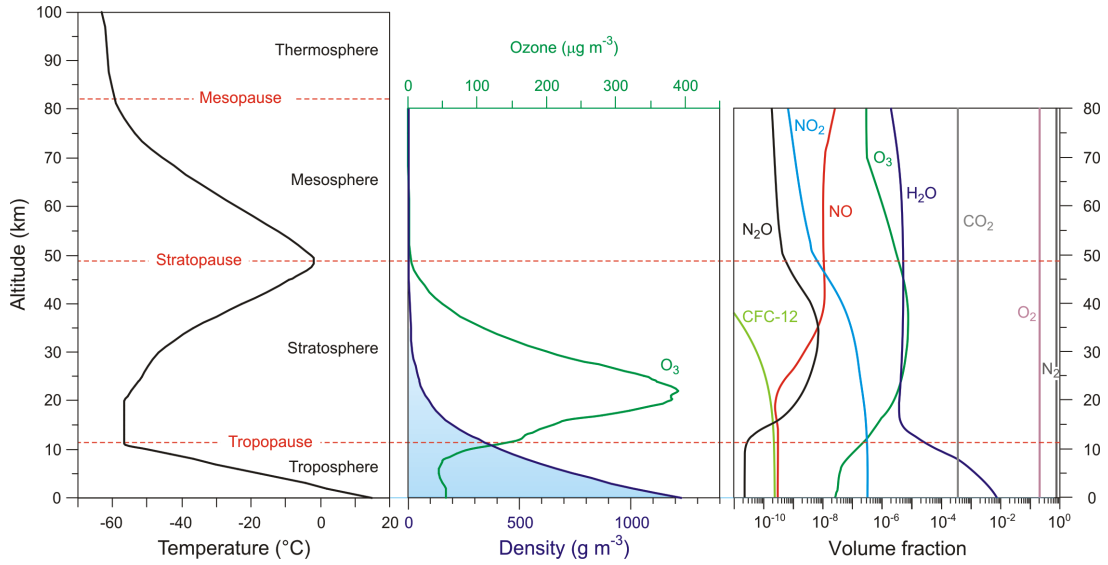

Figure 3: Vertical density profiles of primary atmospheric constituents. While the well-mixed dry gases (molecular nitrogen, N_2, and oxygen, O_2) follow a standard hydrostatic scale height of $H \approx 8$ km, water vapor (H_2O) exhibits a drastically steeper exponential decay with a scale height of $H \approx 2 - 3$ km. Because water vapor concentration is highly temperature-dependent and prone to condensation, the vast majority of precipitable water vapor (PWV) is trapped within the lowest layers of the troposphere. This steep drop-off drives the necessity of placing infrared and sub-millimeter observatories at extreme altitudes. Figure taken from [1].

Instead, it is the **trace and variable constituents** (specifically heteronuclear molecules) that dominate atmospheric opacity. Gases such as carbon dioxide (CO_2) and ozone (O_3) possess complex, asymmetric ro-vibrational modes that create dense forests of absorption lines. Atomic and molecular transitions that cause these absorption features include pure rotational molecular transitions (H_2O, CO_2, O_3), ro-vibrational molecular transitions (CO_2, NO, CO), and electronic atomic and molecular transitions. This atmospheric opacity defines atmospheric transmission windows and bands, where transmission can be significantly reduced by narrow telluric absorption features. However, the most critical and highly variable component for ground-based observational astronomy is water vapor (H_2O).

To measure the amount of water vapor in the air, meteorologists and astronomers rely on several key thermodynamic metrics:

- **Specific Humidity / Mixing Ratio (r):** This is the fractional content of water

[1] https://glossary.periodni.com/glossary.php?en=troposphere

vapor, defined as the mass of H_2O per unit volume divided by the mass of dry air per unit volume. Typically expressed in g/kg, the mixing ratio is highly sensitive to temperature (T), altitude (z), latitude, and time. It is physically bounded by saturation, such that $0 < r \leq r_s(T)$.

- **Relative Humidity (RH):** This is a percentage representing the current water vapor content relative to the atmosphere's maximum capacity to hold water at that specific temperature. It is defined as:

$$\text{RH} = \frac{\text{water vapor content}}{\text{maximum water vapor content for saturation at a given } T}$$

- **Dew Point:** The temperature to which a given air parcel must be cooled to achieve water vapor saturation. In practical observatory operations, monitoring the dew point is strictly enforced to prevent catastrophic condensation on delicate optics. Major facilities mandate dome closures when relative humidity exceeds 80%, and only reopen when levels drop below 70% for sustained periods. Additionally, domes must immediately close if the temperature difference between the coldest part of the telescope structure and the local dew point drops below 2°C.

As illustrated in Figure 3, unlike the well-mixed dry gases that follow a standard hydrostatic scale height of $H \approx 8$ km, water vapor is heavily concentrated in the lower troposphere, possessing a much smaller scale height of roughly $H_{H_2O} \approx 2$ to 3 km.

Astronomers quantify this using **Precipitable Water Vapor (PWV)**, which is the depth of water in a column if all the vapor were condensed to a liquid:

$$\text{PWV} = \frac{1}{\rho_{\text{water}}} \int_0^\infty \rho_{H_2O}(z)\, dz \tag{8}$$

If we establish an observatory at a specific altitude z_0, the total column of PWV can also be expressed by integrating the exponential decay of the mixing ratio $r(z)$ through the remainder of the atmosphere:

$$\text{PWV} \approx \rho_0 \int_{z_0}^\infty r(z) e^{-z/H}\, dz \tag{9}$$

where ρ_0 is the total air density at the observatory's altitude (z_0), and H is the standard atmospheric scale height.

Because the H_2O scale height is so short, building observatories at high altitudes drastically reduces the PWV from ~ 20 mm at sea level to < 1 mm. By bypassing the bulk of the tropospheric inversion layer, these extreme elevations open up otherwise completely inaccessible infrared and sub-millimeter astronomical windows.

2.3 Differential Absorption and Atmospheric Transmittance

The total atmospheric transmittance, T_λ, is the probability that a photon will survive its journey to the detector. It is defined by the line-of-sight integration of the total opacity

κ_λ:

$$T_\lambda = \exp\left(-\int_0^\infty \kappa_\lambda(z)\rho(z)\sec(z)\,dz\right) = e^{-\tau_\lambda \sec(z)} \tag{10}$$

where τ_λ is the **zenith optical depth**. This dimensionless quantity represents the total vertical attenuation integrated directly overhead from the telescope's altitude ($z = 0$) to the top of the atmosphere. It is mathematically defined as the purely vertical component of the integral:

$$\tau_\lambda = \int_0^\infty \kappa_\lambda(z)\rho(z)\,dz \tag{11}$$

The absorption component of κ_λ is fiercely wavelength-dependent, driven by the quantized energy states of the atmospheric molecules. As illustrated in Figure 4, this creates distinct observing windows and cutoffs across the electromagnetic spectrum:

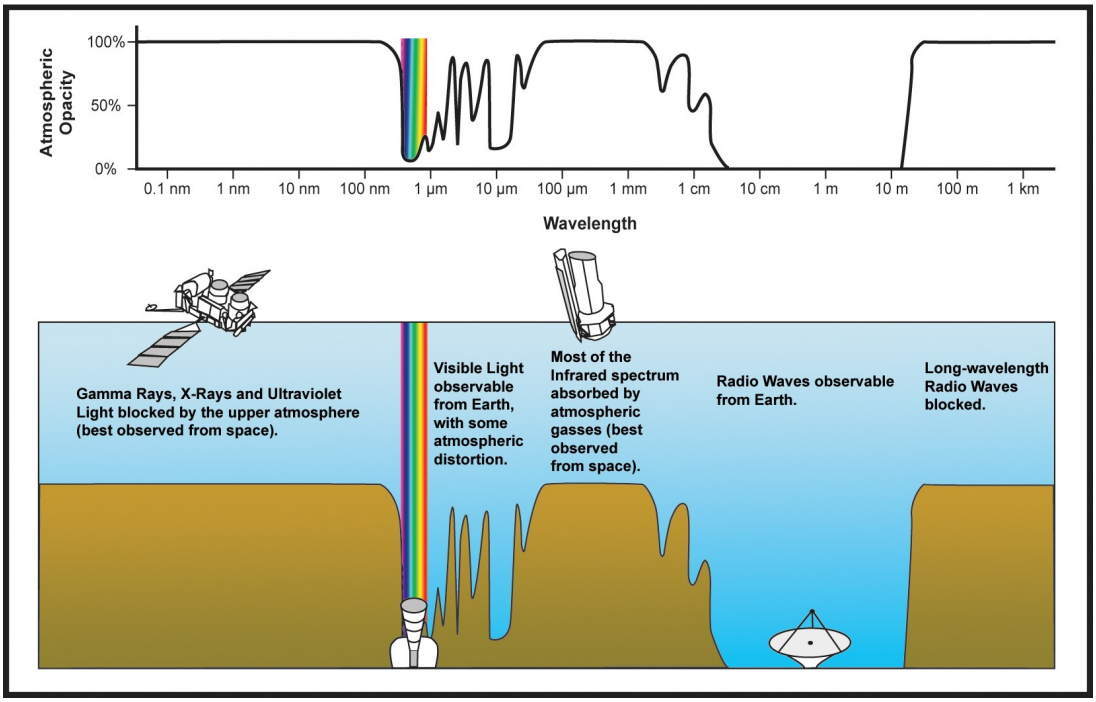

Figure 4: **Atmospheric opacity across the electromagnetic spectrum.** The Earth's atmosphere acts as a highly selective filter for incoming radiation. High-energy photons (gamma rays, X-rays, and extreme ultraviolet) are entirely blocked by the upper atmosphere and ozone layer, while long-wavelength radio waves are reflected by the ionosphere. Ground-based astronomy is therefore restricted to two primary regions: the narrow optical window and the broad radio window. Between these lies the infrared regime, which is heavily characterized by a "picket fence" of deep absorption bands caused by trace atmospheric gases like H_2O and CO_2, necessitating space-based or high-altitude observatories for unhindered observations. Figure taken from [2].

- **High-Energy Cutoff (UV, X-Ray, γ-Ray):** For $\lambda < 100$ nm ($E > 12.4$ eV), N_2 and O_2 are photoionized ($h\nu + O_2 \rightarrow O_2^+ + e^-$). For $200 < \lambda < 300$ nm, the Hartley

[2] https://da.wikipedia.org/wiki/Fil:Atmospheric_electromagnetic_transmittance_or_opacity.jpg

and Huggins bands of Stratospheric Ozone (O_3) completely absorb the near-UV via photodissociation.

- **The Infrared "Picket Fence":** Heteronuclear trace molecules (H_2O, CO_2, O_3) possess dipole moments. They absorb photons to excite quantized vibrational modes coupled with rotational states ($E = E_{\text{vib}} + E_{\text{rot}}$). H_2O creates profound opacity walls at $1.4\mu m$, $1.9\mu m$, and $2.6\mu m$, while CO_2 completely blocks the sky at $4.3\mu m$ and $15\mu m$.
- **The Optical Window:** Between the UV electronic transitions (< 300 nm) and the IR ro-vibrational transitions (> 1000 nm) lies the optical window ($300 - 1000$ nm).

The Ionospheric Plasma Cutoff: While the atmosphere is highly transparent in the radio regime, it becomes completely opaque to very low-frequency radio waves due to the ionosphere. Solar extreme ultraviolet (EUV) and X-ray radiation ionize the upper atmosphere, creating a diffuse plasma characterized by distinct altitude-dependent stratifications, most notably the E and F layers (see Figure 5).

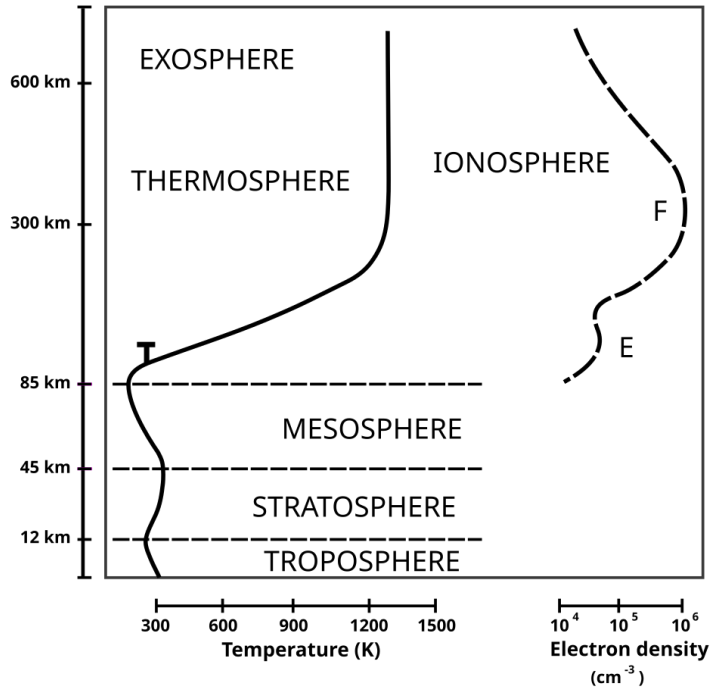

Figure 5: **Vertical profiles of atmospheric temperature and ionospheric electron density.** The neutral atmosphere is defined by its thermal gradient (Troposphere to Thermosphere), while the ionosphere is defined by its free electron concentration (N_e). Notice how the electron density increases sharply with altitude, forming the moderate E layer and peaking significantly in the F layer. Figure taken from [3].

The **E layer** (roughly 90 to 150 km in altitude) is primarily ionized by soft X-rays and far-ultraviolet radiation, sustaining a moderate electron density on the order of 10^4 to

[3] https://en.wikipedia.org/wiki/File:AtmosphereWithIonosphere.gif

10^5 cm^{-3}. Above it lies the **F layer** (150 to over 500 km), which absorbs the bulk of solar EUV radiation and consequently hosts the highest concentration of free electrons in the atmosphere, peaking near 10^6 cm^{-3}. As illustrated in Figure 6 (Left Panel), solar illumination drastically alters this structure: during the day, a lower D layer emerges, and the F layer splits further into the F1 and F2 layers.

Because these distinct layers possess different local electron densities (N_e), they govern exactly which radio frequencies can pass and which are reflected. The refractive index n of such a collisionless plasma is mathematically defined as:

$$n^2 = 1 - \left(\frac{\nu_p}{\nu}\right)^2 \quad \text{where} \quad \nu_p \approx 8980\sqrt{N_e} \tag{12}$$

Here, N_e is the local electron density (in cm^{-3}) and ν_p is the plasma frequency. When the observing frequency ν drops below the plasma frequency (typically around 10 to 20 MHz depending on solar activity), the refractive index becomes purely imaginary.

This effect is highly frequency-dependent (see Figure 6, Right Panel). Lower frequencies are reflected by lower-density layers, while higher frequencies can penetrate further or pass through entirely. For astronomy, this results in the total reflection of incoming extraterrestrial radio waves when $\nu < \nu_p$, placing a hard, fundamental limit on low-frequency ground-based radio observations.

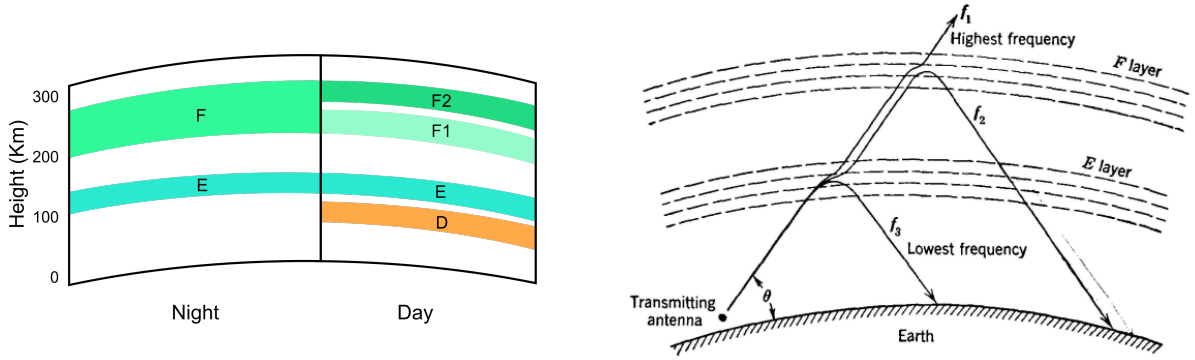

Figure 6: **Ionospheric structure and radio wave propagation.** *(Left Panel)* Diurnal variations in ionospheric stratification. During the day, increased solar radiation induces the formation of the lower D layer and causes the F layer to split into the distinct F1 and F2 layers, while only the E and a single F layer remain at night. *(Right Panel)* Frequency-dependent radio wave interaction. Lower frequencies (f_3) reflect off lower-density layers (like the E layer), medium frequencies (f_2) penetrate deeper to reflect off denser layers (F layer), while high frequencies (f_1) exceeding the maximum plasma frequency ($\nu > \nu_p$) penetrate the ionosphere entirely. By the principle of reversibility, this mechanism prevents low-frequency astronomical radio signals from reaching the ground. Figures taken respectively from [4] and [5].

[4] https://commons.wikimedia.org/wiki/File:Ionosphere_Layers_es.svg#/media/File:Ionosphere_Layers_en.svg
[5] https://www.vias.org/albert_ecomm/aec12_radio_wave_propagation_010.html

2.4 Emission: The Sky Background

The Earth's atmosphere is a prolific emitter across the electromagnetic spectrum, presenting a background that can be many orders of magnitude brighter than the astronomical targets. This emission is not uniform; it is governed by two distinct physical regimes that transition near the K-band ($\sim 2.2\,\mu$m).

- **Airglow (Chemiluminescence):** In the visible and near-infrared (NIR), the background is dominated by *airglow*: photons emitted by atoms and molecules in the upper mesosphere (at altitudes of $\sim$ 85–100 km). This "cold" light is produced by the recombination of species photo-dissociated by solar UV during the day. The most significant contributor is the **hydroxyl radical (OH^-)**, which produces a dense "forest" of ro-vibrational emission lines between 1.0 and 2.2 μm. As illustrated in Figure 7, this dense airglow competes directly with anthropogenic light pollution in the visible regime. Because these lines are discrete, high-resolution spectroscopy ($R > 3000$) can "resolve out" the sky, allowing observations in the dark gaps between OH lines.
- **Thermal Emission:** Beyond $\lambda \approx 2.2\,\mu$m, the non-thermal airglow is overtaken by an exponentially rising thermal continuum. In this regime, the atmosphere behaves as a "greybody" in Local Thermodynamic Equilibrium (LTE) up to an altitude of roughly 60 km. For low optical depths ($\tau \ll 1$), the specific intensity I_λ is modeled by the Planck function $B_\lambda(T)$ at the ambient atmospheric temperature ($T \approx 250$–300 K), scaled by the emissivity ϵ_λ:

$$I_\lambda = \epsilon_\lambda B_\lambda(T_{\rm atm}) \approx (1 - e^{-\tau_\lambda}) B_\lambda(T_{\rm atm}) \tag{13}$$

  where τ_λ is the optical depth. This thermal background is massive; at 10 μm, a ground-based telescope effectively sits inside a glowing furnace, requiring rapid subtraction techniques to prevent detector saturation.

2.4.1 Sky Background for Space-Based Instruments

Space-based facilities, such as the *Hubble Space Telescope* (HST), are free from the atmospheric OH^- airglow and thermal greybody emission that plague ground-based observations. This stark contrast between terrestrial and space-based background limits is plotted in Figure 8 (left panel, 8a). However, these orbiting observatories are still subject to other diffuse background sources, which are decomposed in the right panel (8b):

- **Zodiacal Light:** Sunlight scattered by interplanetary dust in the solar system. This is the dominant background component in the optical and near-IR for space-based observatories. Its intensity depends strongly on the *ecliptic latitude* and the *elongation* (angle from the Sun).
- **Earthshine:** For Low-Earth Orbit (LEO) satellites like HST, sunlight reflected off the Earth's atmosphere can leak into the telescope's baffles, particularly when the target is near the Earth's limb.
- **Geocoronal Emission:** Specifically in the UV, the outermost layers of the Earth's atmosphere (the exosphere) emit resonant scattering lines, most notably Lyman-α

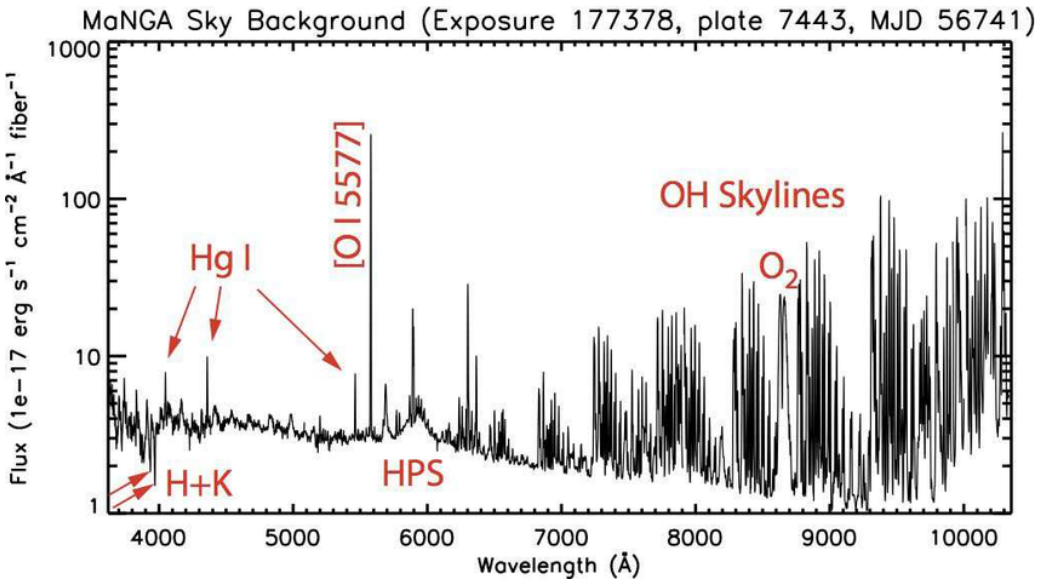

Figure 7: A flux-calibrated night-sky background spectrum from the SDSS-IV MaNGA survey. Shortward of 7000 Å, the spectrum displays discrete mercury ($Hg\,I$) and high-pressure sodium (HPS) lines from anthropogenic light pollution, alongside the natural atmospheric [$O\,I$] 5577 Å line. Longward of 7000 Å, the background is dominated by the dense airglow "forest" of blended OH and O_2 ro-vibrational transitions. The absorption features near 4000 Å are zodiacal Fraunhofer H and K lines, indicating the presence of scattered sunlight in the terrestrial night sky. Figure taken from [5].

(1216 Å) and O I (1304 Å), which contribute to the background even when observing from space.

2.5 Scattering, Refraction & Dispersion

While differential absorption strictly removes photons at specific quantum resonances, scattering continuously redirects photons out of the line of sight across the entire spectrum. Scattering is broadly divided into two regimes based on the dimensionless size parameter $x = 2\pi a/\lambda$, where a is the particle radius and λ is the incident wavelength:

1. **Rayleigh Scattering ($x \ll 1$):** When the scattering particle is significantly smaller than the wavelength of light (e.g., N_2 and O_2 molecules), the process is perfectly elastic. The scattering cross-section is highly chromatic, scaling inversely with the fourth power of the wavelength:

$$\sigma_R(\lambda) \propto \lambda^{-4} \tag{14}$$

Because of this extreme dependence, blue light ($\sim$ 400 nm) is scattered roughly 16 times more efficiently than red light ($\sim$ 800 nm). For observational astronomy, this is the primary driver of **atmospheric reddening**: as celestial objects approach

[6] https://hst-docs.stsci.edu/wfc3ihb/chapter-9-wfc3-exposure-time-calculation/9-7-sky-background#id-9.7SkyBackground-9.7.19.7.1ZodiacalLight,EarthShine,andLOW-SKY

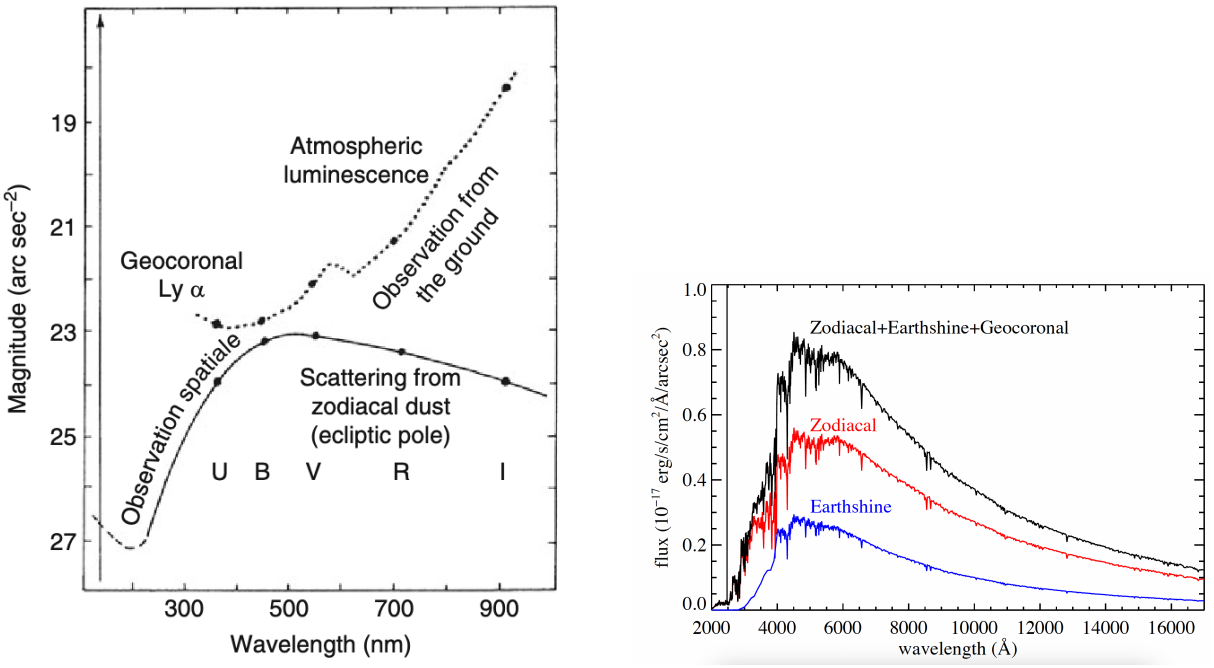

(a) Ground vs. Space Background (b) Space Background Components

Figure 8: Comparison of sky background regimes. Left: The divergence between terrestrial and space-based background magnitudes across standard photometric bands, showing the atmospheric airglow floor for ground facilities. Right: A high-resolution decomposition of space-based background components, identifying the contributions of Zodiacal light, Earthshine, and Geocoronal line emissions (e.g., Lyman-α) as modeled for the WFC3 environment. Figure (a) taken from [1] and (b) adapted from [6].

the horizon, short-wavelength photons are preferentially scattered out of the beam, causing the object's spectrum to artificially shift toward the red.

2. **Mie Scattering ($x \gtrsim 1$):** When the particle size is comparable to or larger than the wavelength (e.g., macroscopic aerosols like water droplets, dust, or pollen), the scattering behavior changes entirely. Mie scattering is highly directional (strongly forward-scattering) and exhibits a much weaker wavelength dependence, roughly scaling as λ^{-1} to λ^0. Because it scatters all visible wavelengths relatively equally, Mie scattering creates a **"grey" extinction component**. This is the physical reason why clouds, fog, and heavy haze appear white or grey rather than blue.

Atmospheric Refraction: As starlight passes through varying density layers of the atmosphere, it bends. The apparent zenith distance of a source is altered significantly. The refraction angle R can be approximated by $R = (n(\lambda) - 1)\tan(\theta)$, requiring all modern telescopes to use robust pointing models to track objects accurately, as visualized in Figure 9.

Atmospheric Dispersion: Because the refractive index of air $n(\lambda)$ varies with wavelength, atmospheric refraction bends blue light more than red light. This differential bending causes broadband point sources to elongate vertically into a rainbow spectrum.

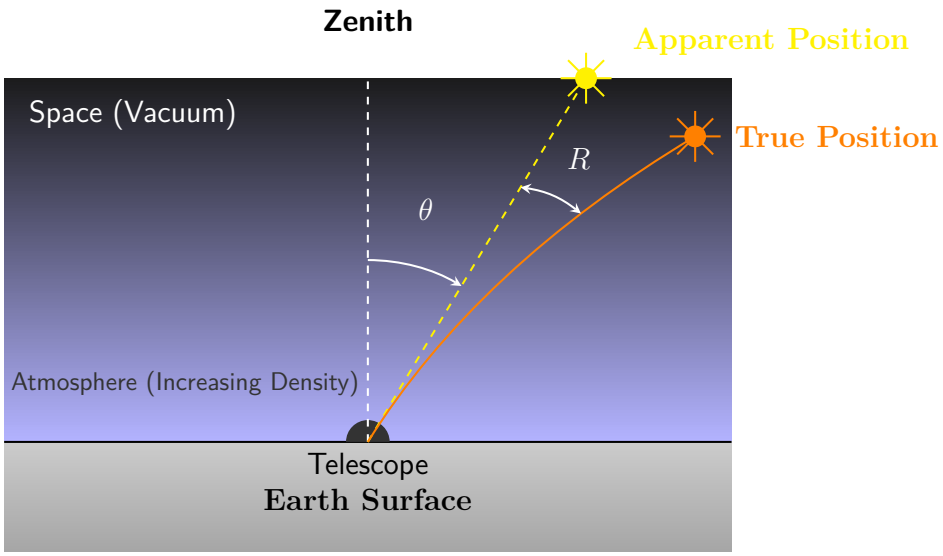

Figure 9: Atmospheric refraction of starlight. As photons enter increasingly dense layers of the Earth's atmosphere, their path bends towards the zenith. This causes the apparent position of the star to be higher in the sky than its true position, separated by the refraction angle R.

This elongation severely degrades the image quality of large, diffraction-limited telescopes, making an Atmospheric Dispersion Corrector (ADC), typically built from dual counter-rotating prisms, a strictly necessary optical component (see Figure 10).

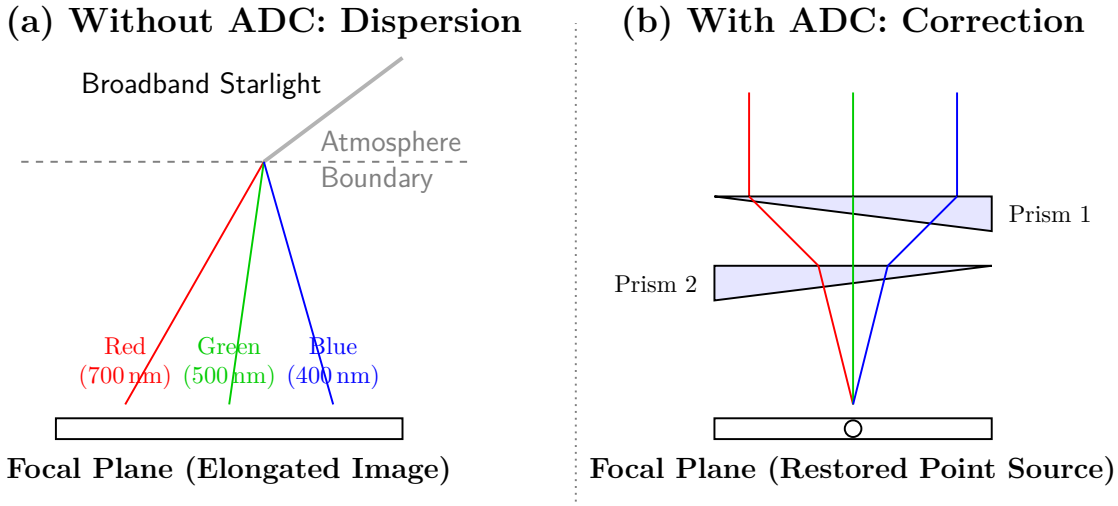

Figure 10: The effect of Atmospheric Dispersion and its correction. **(a)** Differential refraction in the atmosphere bends blue wavelengths more strongly than red, elongating a point source into a vertical spectrum at the focal plane. **(b)** An Atmospheric Dispersion Corrector (ADC) uses counter-rotating prisms with specific chromatic properties to recombine the dispersed rays, restoring diffraction-limited image quality.

Airmass (X) and Total Extinction (Bouguer's Law): To accurately correct for

these combined scattering and absorption effects, we must determine exactly how much atmosphere the light has passed through. This introduces **Airmass (X)**, a fundamental concept in observational astronomy that quantifies the relative optical path length normalized to the zenith.

Assuming a simple plane-parallel model of the Earth's atmosphere, the airmass $X(z)$ is defined by the ratio of the path length at zenith angle z (L) compared to the path length at the zenith (h):

$$X(z) = \frac{L}{h} \tag{15}$$

As illustrated in Figure 11, these lengths form a right triangle with the zenith angle z. From trigonometry, we find $\cos(z) = h/L$, which implies $L = h/\cos(z)$. Substituting this into the ratio yields:

$$X(z) = \frac{h/\cos(z)}{h} = \frac{1}{\cos(z)} = \sec(z) \tag{16}$$

By definition, at the zenith ($z = 0°$), $X = 1$. As a source lowers in the sky, its light passes through a thicker slice of the atmosphere. For example, at $z = 60°$ (which is 30° above the horizon), the light passes through twice as much atmosphere, yielding $X = 2$.

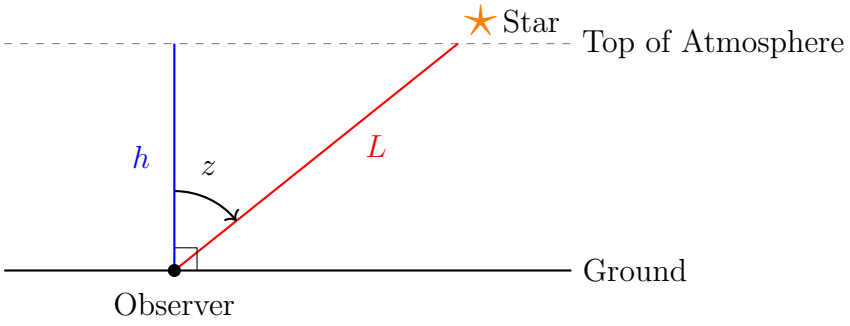

Figure 11: Geometry of the plane-parallel atmosphere. The light travels along path L from the Star, forming a right triangle where $\cos(z) = h/L$. This simplifies to the airmass definition $X(z) = \sec(z)$.

While the plane-parallel approximation of Eq. 16 is highly accurate for objects high in the sky, it begins to fail drastically as objects approach the horizon (typically for $z > 70°$). At these extreme angles, the secant function physically diverges toward infinity. In reality, the physical curvature of the Earth and the refractive downward bending of light become dominant factors, ultimately capping the maximum airmass at the horizon at approximately 38. To calculate the true optical path length at these angles, astronomers utilize complex spherical interpolations, such as the empirical approximation formula derived by [3]:

$$X(\gamma) = \frac{1}{\sin(\gamma) + 0.50572\,(\gamma + 6.07995°)^{-1.6364}} \tag{17}$$

where $\gamma = 90° - z$ is the apparent elevation angle of the target in degrees.

With the path length defined, astronomers convert the physical flux attenuation into the logarithmic magnitude system. This yields **Bouguer's Law**, which states that the

observed magnitude m_λ of a star increases linearly with the airmass:

$$m_\lambda = m_{\lambda,0} + 1.086\tau_\lambda X = m_{\lambda,0} + k_\lambda X \tag{18}$$

where $m_{\lambda,0}$ is the true, extra-atmospheric magnitude, τ_λ is the zenith optical depth, and k_λ is the zenith extinction coefficient. By observing a target at multiple airmasses throughout the night, astronomers can plot m_λ against X and extrapolate the data back to $X = 0$ to find the star's true brightness above the atmosphere.

2.6 Turbulence & Seeing: Kolmogorov Theory

Atmospheric turbulence fundamentally arises when the Reynolds number ($Re = \frac{\rho V L}{\mu}$) of the wind flow exceeds a critical threshold, typically transitioning from laminar to turbulent behavior at $Re \sim 2200$. The most significant constraint on the angular resolution of ground-based facilities is atmospheric *seeing*. This degradation is driven by microscopic temperature fluctuations ($\Delta T \sim 0.01 - 0.1\,\mathrm{K}$) resulting from wind shear and convective mixing. These fluctuations induce localized variations in the refractive index n, effectively turning the atmosphere into a dynamic complex of "lenses" with varying focal lengths. As illustrated in Figure 12, a planar wavefront from a distant star becomes severely corrugated as it traverses these turbulent atmospheric cells.

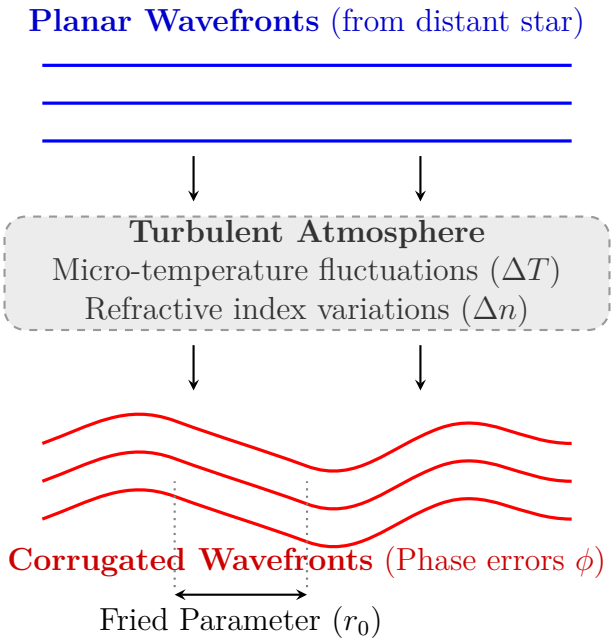

Figure 12: A planar wavefront from a distant star becoming corrugated (aberrated) as it passes through turbulent atmospheric cells. The Fried parameter r_0 characterizes the spatial scale over which the phase error remains relatively coherent.

The statistical behavior of this degradation follows **Kolmogorov turbulence** theory, which assumes energy is injected at a large scale (L_0, the outer scale) and cascades down to a small scale (l_0, the inner scale) where it is dissipated by viscosity. Within this "inertial range", the strength of these optical fluctuations is quantified by the **Refractive Index**

Structure Constant, denoted as $C_n^2(h)$. This parameter measures the variance of the refractive index at a given altitude h; larger values indicate violent atmospheric mixing (poor seeing), while lower values correspond to calm, uniform air. Integrating this vertical turbulence profile from the telescope pupil to the top of the atmosphere yields the total phase structure function:

$$D_\phi(\rho) = 6.88 \left(\frac{\rho}{r_0}\right)^{5/3} \tag{19}$$

where r_0 **is the Fried Parameter** (coherence length), representing the diameter of a circular area over which the RMS phase aberration is approximately 1 radian:

$$r_0(\lambda) = \left[0.423 \left(\frac{2\pi}{\lambda}\right)^2 \sec(z) \int_0^\infty C_n^2(h) dh\right]^{-3/5} \propto \lambda^{6/5} \sec(z)^{-3/5}. \tag{20}$$

The physical manifestation of this turbulence is a function of the ratio D/r_0. As turbulent cells traverse the line of sight (the "frozen flow" Taylor hypothesis), they impart different effects. The turbulence does not change arbitrarily fast but is characterized by a **coherence time** (τ_0). Assuming the frozen turbulent medium passes the telescope aperture at wind speed v, the atmospheric coherence time (or Greenwood delay) is approximately $\tau_0 \approx 0.314\frac{r_0}{v}$. This is the maximum time delay for the RMS wavefront error to be less than 1 radian. Depending on the aperture size relative to r_0, the effects are:

- **Small Apertures ($D \lesssim r_0$):** The aperture samples only a portion of a single turbulent cell. The primary effect is **tip-tilt** (wavefront tilt), causing the image to wander or "dance" intensely in the focal plane while remaining relatively sharp (diffraction-limited).
- **Large Apertures ($D \gg r_0$):** The telescope spatially integrates over numerous uncorrelated turbulent cells simultaneously. This superposition of multiple instantaneous PSFs blurs the point source into a broad, time-averaged **seeing disk**. This transition from the theoretical diffraction limit to an atmospherically degraded profile is visually compared in Figure 13.

For a large professional telescope, the Long-Exposure PSF evolves into a Gaussian-like profile with a Full-Width at Half-Maximum (FWHM) determined by the atmosphere rather than the optics:

$$\text{FWHM}_{\text{seeing}} \approx 0.98\frac{\lambda}{r_0} \propto \lambda^{-1/5} \sec(z)^{3/5} \tag{21}$$

Note the weak dependence on wavelength ($\lambda^{-1/5}$); while r_0 improves significantly in the infrared ($r_0 \propto \lambda^{1.2}$), the actual seeing disk only shrinks slightly.

Because r_0 restricts the resolution, several high-speed observational techniques have been developed to overcome the seeing limit by "freezing" the wavefront within its short coherence time (τ_0). These include hardware-based real-time Adaptive Optics (AO) and post-processing methods such as **Speckle Interferometry** (e.g., bispectrum analysis), Shift-and-Add, and Lucky Imaging.

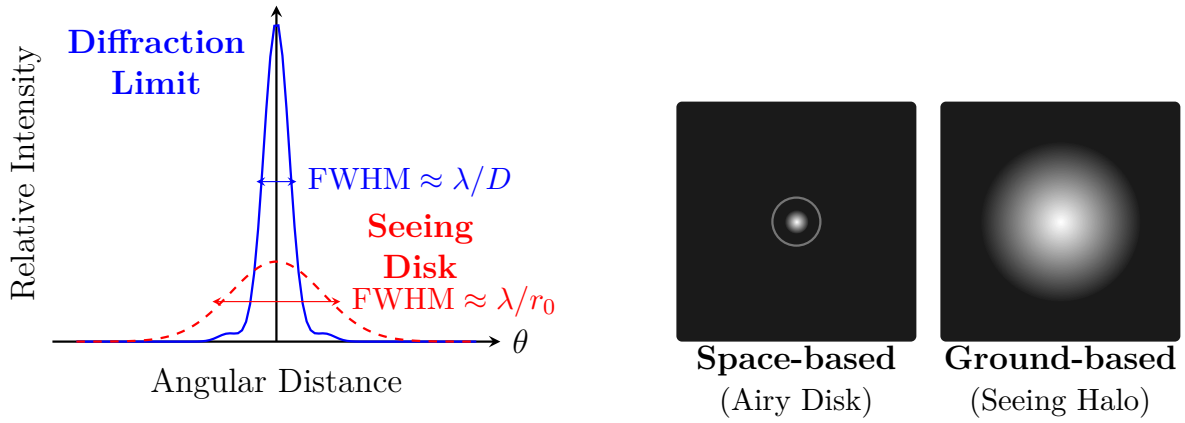

Figure 13: The practical effect of atmospheric turbulence on a point source. **Left:** The 1D intensity profiles demonstrating how the sharp diffraction-limited core (blue) is smeared into a broad seeing disk (red dashed). Energy is conserved, resulting in a drastic loss of peak intensity. **Right:** A simulated 2D view on a detector, comparing the theoretical Airy pattern (with its diffraction ring) to the heavily degraded atmospheric PSF.

Scintillation and Aperture Averaging: A distinction must be made between seeing (phase errors) and **Scintillation** (amplitude errors). Scintillation is the rapid temporal fluctuation of total observed flux ("twinkling"), primarily caused by high-altitude turbulence ($\sim 10\,\text{km}$) near the jet stream.

As the corrugated wavefront propagates to the ground, Fresnel diffraction creates an intensity pattern of "flying shadows" across the pupil. While small apertures sample these intensity peaks and valleys individually (causing high photometric noise), large mirrors ($D \gg 20\,\text{cm}$) perform **aperture averaging**, integrating over thousands of these patterns simultaneously. As depicted in Figure 14, this spatial integration effectively smooths out the high-amplitude variations. Consequently, for professional 8m-class telescopes, scintillation noise is often reduced to the millimag level, making them superior for high-precision photometry of bright targets.

2.7 Criteria for Astronomical Site Selection

Given the severe degradative effects of the atmosphere, minimizing its impact requires rigorous geographic site selection for new observatories. Premium ground-based observatories must satisfy several stringent physical criteria:

1. **High Altitude and Inversion Layers:** Observatories are placed at extreme elevations (e.g., Mauna Kea at 4,200 m or the Chajnantor Plateau at 5,000 m) to reside above the atmospheric boundary layer and the vast majority of precipitable water vapor, effectively opening the infrared and sub-millimeter observing windows. Furthermore, placing telescopes on peaks above the local thermal inversion layer ensures that pervasive cloud cover remains permanently trapped below the observatory (see Figure 15).
2. **Laminar Airflow and Local Topography:** Ideal sites are isolated coastal peaks

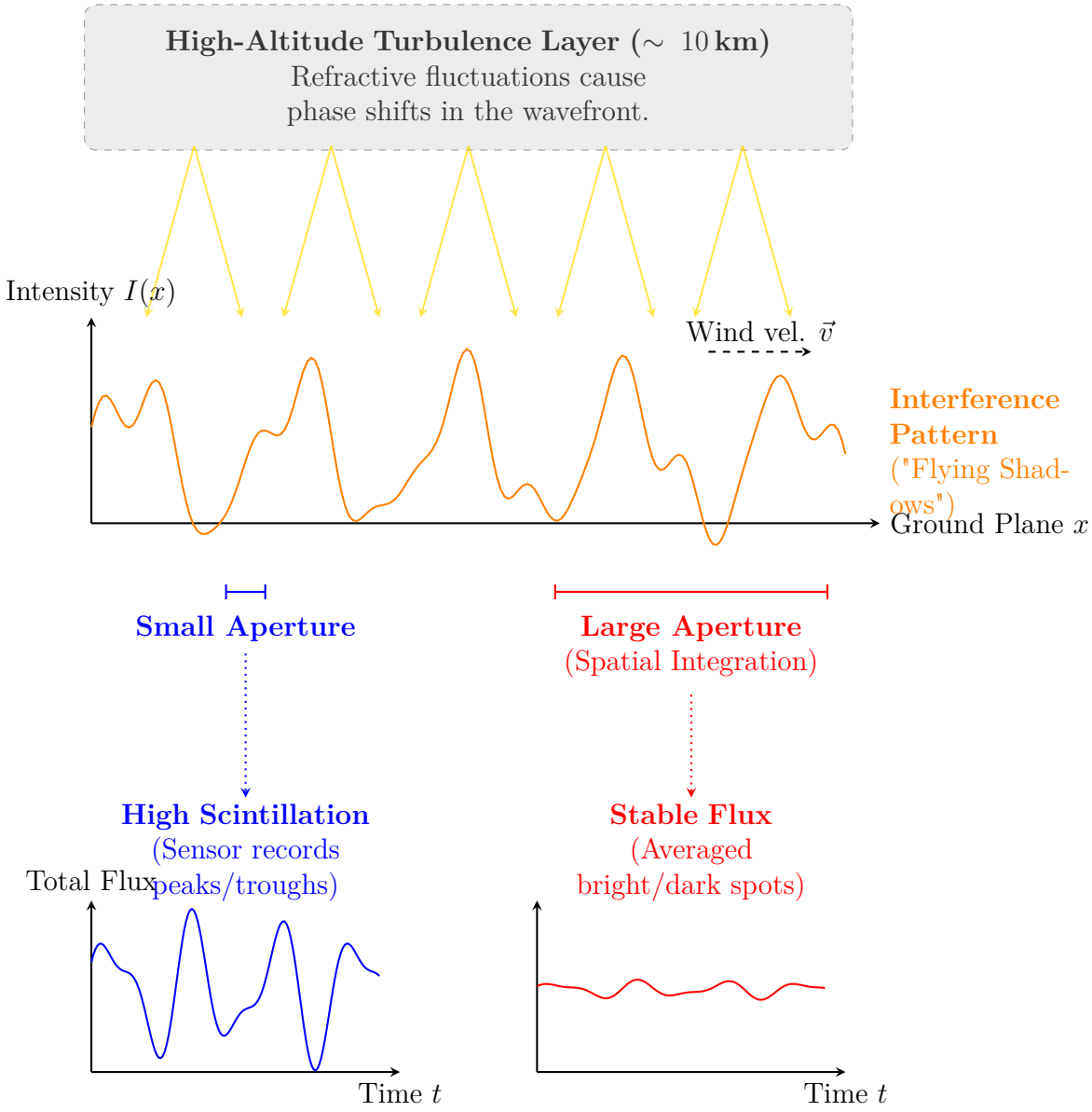

Figure 14: The mechanism of aperture averaging. A high-altitude turbulent layer creates an interference pattern of bright and dark spots on the ground. A small aperture (left) fits inside these spots, causing high-amplitude scintillation (twinkling) as the wind moves them. A large aperture (right) spans many spots, averaging out the variations to record a stable flux.

or oceanic islands where prevailing winds cross thousands of miles of flat ocean before reaching the mountain. The specific local relief and topography directly surrounding the observatory play a dominant role in inducing mechanical turbulence, as illustrated in Figure 16. Solitary, smooth-sloped peaks are highly desirable because they promote laminar, non-turbulent airflow, minimizing local variations in the refractive index structure constant (C_n^2) and resulting in superb intrinsic seeing. Additionally, local weather directly dictates operations; even at ideal sites,

sustained wind speeds exceeding operational thresholds (typically 14 to 20 m/s, depending on dome design) mandate immediate closure to protect instruments from severe wind-shake.

3. **Absence of Anthropogenic Interference:** Sites must be strictly protected from human light pollution to preserve the natural sky background limit, and from anthropogenic radio frequency interference (RFI) for radio arrays.

When ground-based site selection is physically insufficient to overcome atmospheric opacity, thermal background emission, or seeing limits (e.g., for X-ray, Gamma-ray, or far-infrared astronomy), the only mathematical recourse is to bypass the atmospheric propagation medium entirely. This is achieved by placing observatories in the stratosphere using high-altitude balloons (> 30 km) and aircraft (> 12 km), or by launching them fully into space (e.g., Chandra or Spitzer).

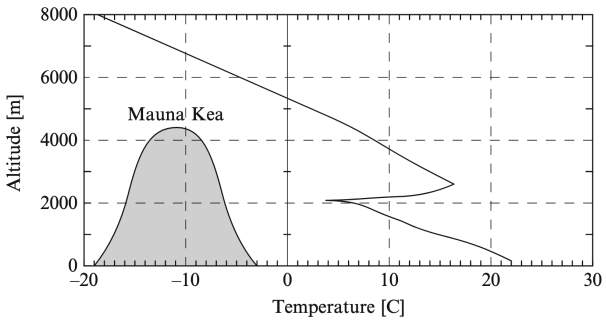

Figure 15: A high-altitude astronomical site located successfully above the tropospheric cloud deck and thermal inversion layer. This altitude versus temperature plot illustrates a prominent subsidence inversion layer near Mauna Kea, Hawaii. The inversion, characterized by a temperature increase with height between approximately 2000 and 4000 meters, results from the adiabatic heating of air within the descending branch of the regional Hadley cell circulation. Figure taken from [1].

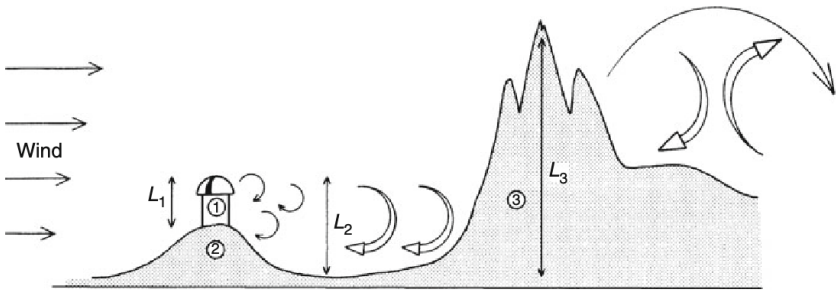

Figure 16: Generation of atmospheric turbulence by varying obstacles. The external scales of turbulence (L_1, L_2, L_3) correspond directly to the size of the structures creating them—from a small observatory dome (1) and a hill (2) to a large mountain (3). This schematic highlights why upwind topography must be evaluated when choosing an astronomical site, as the resulting temperature fluctuations and slowly damping eddies significantly degrade seeing conditions. Figure taken from [1].

References

[1] Léna, P., Rouan, D., Lebrun, F., Mignard, F., & Pelat, D. (2012). *Observational Astrophysics* (3rd ed.). Springer.

[2] Chromey, F. R. (2010). *To Measure the Sky: An Introduction to Observational Astronomy*. Cambridge University Press.

[3] Kasten, F., & Young, A. T. (1989). Revised optical air mass tables and approximation formula. *Applied Optics*, 28(22), 4735-4738.

[4] Rybicki, G. B., & Lightman, A. P. (1986). *Radiative Processes in Astrophysics*. Wiley-VCH.

[5] Law et al. (2016). *The Data Reduction Pipeline for the SDSS-IV MaNGA IFU Galaxy Survey*. Astronomical Journal, 152(4). *(Source of the flux-calibrated night-sky background spectrum used to illustrate the atmospheric airglow "forest" and anthropogenic light pollution limits.)*

These course notes were refined with the assistance of Gemini 3.1 Pro. Unless otherwise cited, all figures were generated using this tool.
Last updated: March 20, 2026